의학박사 학위논문

Assessment of hepatic steatosis using quantitative ultrasound (QUS) in nonalcoholic fatty liver disease

비알코올성 지방간 환자에서 정량적 초음파 영상 지표의 개발 및 지방간 진단능 평가

2021년 2월

서울대학교 대학원

의학과 영상의학 전공

전 선 경

의학박사 학위논문

Assessment of hepatic steatosis using quantitative ultrasound (QUS) in nonalcoholic fatty liver disease

비알코올성 지방간 환자에서 정량적 초음파 영상 지표의 개발 및 지방간 진단능 평가

2021년 2월

서울대학교 대학원

의학과 영상의학 전공

전 선 경

Assessment of hepatic steatosis using quantitative ultrasound (QUS) in nonalcoholic fatty liver disease

지도교수 이 정 민

이 논문을 의학과 박사 학위논문으로 제출함

2020년 10월

서울대학교 대학원

의학과 영상의학 전공

전 선 경

전선경의 의학박사 학위논문을 인준함

2021년 1월

위 원 장 이 재 영 (인)

부위원장 이 정 민 (인)

위 원 김 윤 준 (인)

위 원 김 세 형 (인)

위 원 박 희 선 (인)

Abstract

Assessment of hepatic steatosis using quantitative ultrasound (QUS) in nonalcoholic fatty liver disease

Sun Kyung Jeon

Department of Radiology, College of Medicine

The Graduate School

Seoul National University

Purpose: To investigate the diagnostic performance of quantitative ultrasound (QUS) parameters for the assessment of hepatic steatosis in patients with nonalcoholic fatty liver disease (NAFLD) using magnetic resonance imaging proton density fat fraction (MRI-PDFF) as the reference standard.

Materials and methods: In this single-center prospective study, 120 patients with clinically suspected NAFLD were enrolled between March 2019 and January 2020. Participants underwent ultrasound (US) examination for radiofrequency (RF) data acquisition and chemical shift-encoded liver MRI for PDFF measurement. Using the RF data analysis, attenuation coefficient (AC) at tissue attenuation imaging (TAI) and scatter-distribution coefficient (SC) at tissue scatter-distribution imaging (TSI) were measured. Correlation between the QUS parameters (AC and SC) and MRI-PDFF was evaluated using Pearson correlation coefficients. Diagnostic performance of AC at TAI and SC at TSI for detecting hepatic steatosis (MRI-PDFF ≥5%) and hepatic fat content ≥10% (MRI-PDFF ≥10%) were assessed by

receiver operating characteristic (ROC) analysis. Significant clinical or imaging factors associated with AC and SC were analyzed using linear regression analysis.

Results: Participants were classified with MRI-PDFF <5% (n=38), 5-10% (n=23), and ≥10% (n=59). AC at TAI and SC at TSI were significantly correlated with MRI-PDFF (r=0.659 and 0.727, P<0.001 for both). For detecting hepatic steatosis and hepatic fat content ≥10%, the area under the ROC curves (AUCs) of AC at TAI were 0.861 (95% confidence interval [CI]: 0.786-0.918) and 0.835 (95% CI: 0.757-0.897), and of SC at TSI were 0.964 (95% CI: 0.913-0.989) and 0.935 (95% CI: 0.875-0.972), respectively. In multivariate linear regression analysis, MRI-PDFF was an independent determinant of AC at TAI and SC at TSI.

Conclusion: AC at TAI and SC at TSI derived from quantitative US RF data analysis yielded a good correlation with MRI-PDFF and provided good performance for detecting hepatic steatosis and assessing its severity in NAFLD.

Keywords: Ultrasonography, Liver, Fatty liver, Quantitative imaging, Nonalcoholic fatty liver, Hepatic steatosis

Student Number: 2019-34541

CONTENTS

List of Tables

List of Figures

‘

INTRODUCTION

Nonalcoholic fatty liver disease (NAFLD) affects approximately a quarter of the human population worldwide, with the earliest and characteristic histological feature being hepatic steatosis (1). NAFLD may progress to nonalcoholic steatohepatitis (NASH), an advanced form found in 20% of adults with NAFLD (2, 3), and NASH is a leading cause of liver transplantation as it can contribute to the development of fibrosis, cirrhosis, and hepatocellular carcinoma (2, 4). Although liver biopsy is the current reference standard for diagnosing NAFLD, owing to its invasiveness and possibility of sampling error, a noninvasive technique is required for assessing hepatic steatosis (5).

Chemical shift-encoded magnetic resonance imaging (MRI) based proton density fat fraction (PDFF) and magnetic resonance spectroscopy (MRS) are accurate and reproducible for liver fat quantification, and used as the validated reference standards in many clinical trials for NAFLD (6-8). Despite their strengths, MRI-PDFF and MRS are not routinely available or cost-effective for clinical screening of NAFLD. In this context, ultrasound (US) could be a promising tool as it is noninvasive, widely available, and cost-effective for the evaluation of hepatic steatosis (9). B-mode US imaging, based on the amplitude of the envelope of beam-formed radiofrequency (RF) signals, is frequently used clinically for the assessment of hepatic steatosis (10). However, conventional B-mode US examination is limited due to its subjectivity, operator dependency, and low sensitivity for mild steatosis (11). The controlled attenuation parameter (CAP), a measurement of ultrasonic attenuation vibration obtained in transient elastography

(TE), has been suggested as an alternative due to its advantage of being inexpensive and relatively widely available (12). However, CAP cannot provide B-mode US images and its values can be influenced by several covariates including body mass index (BMI) and diabetes (1).

Recently, increasing attenuation has been paid to quantitative US (QUS) techniques from RF data analysis as a promising tool for tissue characterization. As opposed to B-mode images, raw RF data contain frequency-dependent information of the US signal, which provides additional diagnostic value (13). Recent studies have demonstrated that some quantitative parameters from the RF data analysis reflecting the backscatter or attenuation of US beam correlated with hepatic steatosis grades (10, 14-16). However, little is known about the diagnostic performance of RF data-driven parameters for hepatic steatosis in patients with NAFLD.

Therefore, the purpose of our study was to investigate the diagnostic performance of quantitative US parameters for the assessment of hepatic steatosis in patients with NAFLD.

I. Pilot study: the investigation of quantitative US parameters

MATERIALS AND METHODS

This study consisted of two main parts. The first part was a pilot study to investigate appropriate quantitative US parameters for assessing hepatic steatosis. For the pilot study, a retrospective analysis of data obtained from a prospective study (ClinicalTrials.gov identifier: NCT03047707) was performed. The data from patients with chronic liver disease was analyzed using controlled attenuation parameter as the reference standard. The second part was the main study as a single-center prospective study to evaluate the diagnostic performance of quantitative US parameters for assessing hepatic steatosis in patients with NAFLD using MRI-PDFF as the reference standard (ClinicalTrials.gov identifier: NCT04180631). Both studies (pilot study and main study) were approved by institutional review board of Seoul National University Hospital, and written informed consent was obtained from all participants.

Study population

The study population of pilot study was a subgroup of a prospective multi-center study which primarily aimed to evaluate the performance of a point shear-wave elastography (SWE) for hepatic fibrosis (17)(ClinicalTrials.gov identifier: NCT03047707). In that study, participants were enrolled from May 2017 to April 2018 and underwent both B-mode US with point SWE and TE. Its inclusion

criteria were i) patients with chronic liver disease or liver cirrhosis, or patients scheduled to undergo hepatectomy for liver disease or liver donation, or healthy volunteer, and ii) age ≥18 years old. Patients were excluded if they had i) obstructive cholestasis, ii) high serum aspartate aminotransferase and/or alanine aminotransferase (>5 times the upper normal limit) within 3 months, iii) right heart failure or liver congestion, iv) previous liver surgery, and v) infiltrative liver disease. Among them, data from those who had reliable CAP measurements within the 2-week interval from the B-mode US were selected for the analysis in this study.

B-mode US imaging with RF data

All B-mode US examinations were performed with a diagnostic US system (RS80; Samsung Medison, Co. Ltd.) using a convex probe (CA1-7A). Before B-mode US, participants were requested to fast for at least four hours. Using a predefined preset with S-Harmonic™ mode (pulse inversion + coded harmonic imaging), B-mode images were obtained during a breath-hold with a fixed setting of time-gain compensation, and their RF data were automatically recorded. Scan planes included a right intercostal plane near the level of the hepatic hilum.

During the B-mode US examination, the visual score of hepatic steatosis was recorded by the operator. The visual score of hepatic steatosis was graded as follows: score 0, no; 1, mild; 2, moderate; and 3, severe steatosis) by referring to Hamaguchi's scoring system (18). This uses the following US features of hepatic steatosis: bright liver, increased hepatorenal echo contrast, deep attenuation, and vessel blurring. This uses the following US features of hepatic steatosis: bright liver, increased hepatorenal echo contrast, deep attenuation, and vessel blurring.

Measurement of quantitative US parameters from RF data analysis

Quantitative US parameters of the liver parenchyma, including tissue attenuation imaging parameter (TAI-p) and tissue scatter-distribution imaging parameter (TSI-p) were derived from RF data. TAI-p indicates the slope of the US center frequency downshift with a depth that can be used to estimate acoustic attenuation (19), and TSI-p indicates the average Nakagami parameters of the ROI reflecting the local concentration and arrangement of US scatterers (19, 20). The theoretical backgrounds of those parameters and details on how to create the parametric maps are given in the Appendix 1. Texture features including histogram-based 1st order statistics (mean, standard deviation, skewness, kurtosis) and gray level co-occurrence matrix (GLCM) features (auto-correlation, sum-average, sum-variance, contrast, sum-entropy), were also derived from RF data (21).

By analyzing RF data using an in-house program developed MATLAB R2015a (MathWorks, Inc.), maps of quantitative parameters were generated. With reference to B-mode image, a rectangular region-of-interest (ROI) (about 2cm in width × 4cm in height) or an annulus-sector ROI (about 2cm in inner arc length × 4cm in side length) was positioned in the liver parenchyma in the map of each parameter. ROIs were positioned avoiding large vessels, focal lesions, and reverberation artifacts beneath the liver capsule.

TE with CAP

Using TE (Fibroscan®; Echosens), CAP (in dB/m), and LSM (in kPa) were measured with an M probe according to the manufacturer's recommendations. For

each participant, medians of 10 valid measurements were regarded as the representative of CAP and LSM, respectively (22). They were regarded to be reliable when 10 valid measurements with an interquartile range (IQR) <40 dB/m for CAP (23) and IQR/median ≤30% for LSM (24)

CAP values were used to determine hepatic steatosis grades by applying reference values suggested in a previous study (22): 0-250 dB/m for S0 (no steatosis), >250 dB/m for ≥S1 (mild steatosis), >299 dB/m for ≥S2 (moderate steatosis), and >327 dB/m for S3 (severe steatosis). LSM values on TE were used to determine hepatic fibrosis grades by applying the cut-offs suggested in a previous study (25): 0-7.1 kPa for ≤F1 (no or mild fibrosis), >7.1 kPa for ≥F2 (significant fibrosis), >9.5 kPa for ≥F3 (severe fibrosis), and >12.5 kPa for cirrhosis (F4).

Statistical analysis

Visual scores and quantitative parameters were correlated with CAP-based steatosis grades using the Spearman's correlation analysis. Spearman's correlation coefficient (rho) was interpreted as follows: |rho|>0.5, strong; |rho|=0.3-0.5, moderate; and |rho|<0.3, week correlation (26). As the Kolmogorov-Smirnov test revealed that the visual score, AC at TAI, and texture parameters were not normally distributed, US parameters of different steatosis grades were compared with the Kruskal-Wallis test followed by Dunn's posthoc test without the assumption of a normal distribution of data. In Dunn's posthoc test, a Bonferroni-adjusted P-value less than 0.017 (0.05/3) was considered to be statistically significant as three pairwise comparisons between adjacent grades were performed.

Univariate and multivariate linear regression analyses were performed to evaluate significant determinants of TSI-p and TAI-p, respectively. Statistical analyses were performed using MedCalc 16.4.1 (MedCalc Software) and SPSS 25.0 (IBM corp.). A P-value of less than 0.05 indicated a statistical significance except for the aforementioned pairwise comparison tests.

RESULTS

Study population

Of the 249 participants initially enrolled, six participants with unreliable CAP measurements were excluded from the analysis. Therefore, a total of 243 participants (171 males; age, mean ± standard deviation [SD], 55 ± 13 years old; and body mass index [BMI], mean ± SD, 25 ± 4 kg/m^2) were finally included. Patients' characteristics are summarized in Table 1. The majority had chronic liver diseases (82.7%, 201/243), with the most common cause being chronic hepatitis B (47.7%, 116/243). Based on the CAP values, patients were categorized as having S0, S1, S2, and S3 in 152, 54, 14, and 23, respectively. The number of patients having ≥S1, ≥S2, and S3 were 91 (37.4%), 37 (15.2%), and 23 (9.5%), respectively. None of the patients showed unreliable results in LSM, and 98 patients (40.3%) were categorized as having ≥F2 based on TE results.

Correlation of US parameters with hepatic steatosis grades

TAI-p and TSI-p showed strong negative and positive correlation with steatosis grades (rho = -0.617 and 0.593, respectively, P<0.001 for both), while visual score showed a moderate correlation (rho = 0.352, P<0.001). Of nine texture features, standard deviation, skewness, contrast, sum-entropy showed weak to moderate negative correlations (rho = -0.350 to -0.227, Ps <0.001), while the other five texture features and didn't show a significant correlation with hepatic steatosis grade (Ps >0.05). So, quantitative US parameters-related further analysis was performed using TAI-p and TSI-p.

Diagnostic performances of US parameters for hepatic steatosis grades

For the prediction of ≥S1, ≥S2, and S3, TSI-p showed AUCs of 0.827, 0.914, and 0.917, respectively. TAI-p showed AUCs of 0.844, 0.914, and 0.909, respectively (Table 2). Both TAI-p and TSI-p and TAI-p showed significantly higher AUCs than the visual score for diagnosing ≥S1 or ≥S2 (Ps≤0.003). For the diagnosis of S3, both TSI-p and TAI-p also showed higher AUCs than the visual score with or without statistical significance (Ps≤0.029) (Table 3).

Clinical and laboratory determinants of TSI-p and TAI-p

In the univariate linear regression analysis, BMI, skin-liver capsule distance measured on B-mode US, alanine aminotransferase, and CAP-based steatosis grade were significant factors affecting TAI-p. Additionally, BMI, TE-based fibrosis grade, and CAP-based steatosis grade were significant factors affecting TSI-p. In the multivariate analysis, the steatosis grade was an independent determinant for TAI-p with a negative relationship (P<0.001). In addition, the fibrosis grade and steatosis grade were independent determinants for TSI-p showing negative and positive relationships (P=0.034 and <0.001), respectively. (Table 4).

II. Main study: diagnostic performance of quantitative US parameters in NAFLD

MATERIALS AND METHODS

Study population

Between March 2019 and January 2020, 124 participants who met the eligibility criteria and gave written informed consent were initially enrolled in the main study. The inclusion criteria were as follows: a) age 18 years or older, b) patients referred to the radiology department for ultrasonographic evaluation of the liver because of known or suspected NAFLD or those scheduled to undergo hepatectomy for liver donation. Exclusion criteria were as follows: a) presence of clinical, laboratory, or histological evidence of liver disease other than NAFLD; b) excessive alcohol consumption (≥14 and ≥7 drinks per week, for males and females, respectively); c) the use of hepatotoxic or steatogenic medication; d) previous liver surgery; e) contraindication for MRI; and f) missing MRI or quantitative US data. After excluding patients who had withdrawn consent (n=1) and those with deviations in the data collection protocol (n=3), a total of 120 participants (75 men and 45 women; mean age, 49.1 years ± 12.6 [standard deviation, SD]; age range, 20-73 years) were finally included in this study (Fig. 1).

US data acquisition

For each participant, B-mode liver US examination was performed using a US system (RS 85A, Samsung Medison, Co. Ltd., Seoul, Korea) with a convex probe (CA1-7A) by one of the three abdominal radiologists (I.J., S.K.J., and S.J.P. with more than 6 years of experience in abdominal US examinations) who were blinded to the results of other studies. All participants were requested to fast for at least 4 h prior to the US examinations. Each participant underwent two same-day sessions of examination to assess the reproducibility of the measurements of quantitative US parameters.

During each session of US examination, a radiologist made six data acquisitions at the same location in the right lobe of the liver by using a right intercostal plane near the hepatic hilum. During the data acquisitions, participants were positioned in the supine position with the right arm at maximum abduction. Each B-mode image was obtained during a breath-hold with a fixed set of time-gain compensation and position of focus, and its RF data were automatically recorded.

During the B-mode US examination, the visual score of hepatic steatosis was recorded by the operator as follows: 0, no steatosis; 1, mild steatosis; 2, moderate steatosis; and 3, severe steatosis by referring to Hamaguchi's scoring system using the following features: bright liver, increased hepatorenal echo contrast, deep attenuation, and vessel blurring (18). In addition, all stored B-mode US images were reviewed by an independent reviewer (J.P., with 3 years of experience in abdominal US examinations), and visual scores of hepatic steatosis were evaluated. During the B-mode US, skin-to-liver capsular distance (mm) was also measured by the operator.

Quantitative US parameter measurement

From the results of the pilot study, two quantitative US parameters were evaluated. For the clinical application, the values of previous quantitative US parameters were modified. The modified quantitative US parameters were attenuation coefficient (AC) at TAI and scatter-distribution coefficient (SC) at TSI. As TAI-p (center frequency shift) were presented as a negative value, AC at TAI were derived from the following equation to be presented as a positive value: $\mathrm{AC}\ (dB/cm/MHz) = -\frac{8.686}{4\sigma^2} \cdot \frac{df_c(z)}{dz}$, where z is the depth of the region of interest from the transducer, σ^2 is the variance of the transmit pulse, and $\frac{df_c(z)}{dz}$ is the center frequency shift (TAI-p). SC at TSI was defined as TSI-p (Nakagami parameter) x 100.

Two quantitative US parameters, including the attenuation coefficient (AC) at TAI and scatter-distribution coefficient (SC) at TSI, were computed from the RF data by using an in-house program developed in MATLAB R2015a (MathWorks, Inc., Natick, MA, USA). By analyzing the RF data, color-coded maps of both AC at TAI and SC at TSI of the corresponding B-mode images were generated (Fig. 2). One radiologist (S.K.J.) placed annulus-sector region-of interests (ROIs) (about 2 cm in inner arc length × 4 cm in side length) on TAI and TSI maps of the liver parenchyma by carefully avoiding large vessels, focal lesions, and reverberation artifacts under the liver capsule. In cases where blood vessels were unavoidable during ROI placement, areas of vessels were excluded from the calculation of AC at TAI and SC at TSI, and those areas were presented as vacancies on TAI and TSI maps. Measurements of quantitative US parameters were performed without knowing the MRI-PDFF results. For each quantitative US parameter, the six

measurements per examination were averaged to yield a single value. The results of the two sessions were used for reproducibility analysis; however, only the first session in each participant was used for steatosis assessment as the representative value.

Liver stiffness measurement at shear-wave elastography (SWE)

Point SWE was performed using an intercostal approach in accordance with the recommendations of current international guidelines for point US shear-wave elastography (27). With the reference to B-mode image, ROIs were placed in the right lobe at a depth of approximately 20-40 mm from the liver capsule. The SWE measurements were expressed in kilopascals (kPa) with an automatically calculated RMI, which demonstrated the reliability of each measurement (28), with the RMI ≥0.4 being considered acceptable according to the manufacturers' recommendations. Ten consecutive measurements with an RMI ≥0.4 and an interquartile range (IQR)/median (Med) ≤ 30% were obtained, and the median value was used as a representative value.

MRI-PDFF and MR elastography

All participants underwent chemical shift-encoded liver MRI with MR elastography (MRE) examinations using a 3.0-T MR scanner (Skyra; Siemens Healthineers, Erlangen, Germany). For PDFF, complex-based chemical shift-encoded water-fat reconstruction techniques were used with six two-dimensional (2D) gradient-recalled-echo (GRE) images, an imaging matrix of 256X192, and a slice thickness of 3 mm. To minimize T1 bias between fat and water, a low flip

angle (4°) was applied (29). PDFF maps were reconstructed automatically using the vendor's algorithm with T2* correction calculated from signal decay and a multi-peak fat model (30).

Blinded to the result of quantitative US results, one abdominal radiologist (S.K.J.) manually placed circular ROIs in each of the nine Couinaud liver segments on the PDFF map of each participant. Each ROI with a diameter of 1 cm was placed near the center of each segment with an effort to avoid large vessels, focal lesions, and artifacts. Nine ROIs were averaged and used as the reference standard for hepatic fat content (31). The primary outcome was the presence of hepatic steatosis, defined as MRI–PDFF ≥ 5% (14, 32). In addition, detecting hepatic fat content ≥ 10%, defined as MRI-PDFF ≥ 10%, was the secondary outcome of our study (14, 33).

MRE was also performed using a 2D GRE sequence in all participants in the supine position with 60 Hz vibration applied to the abdominal wall. Four sections were acquired in four consecutive breath-holds. By using a direct inversion algorithm, a confidence mask were automatically generated from the scanner, and superimposed to a MR elastogram (34). Liver stiffness (LS) was measured by one abdominal radiologist (S.K.J.) by drawing a freehand ROI in each section, excluding the large vessels, fissures, or focal liver lesions (35). LS values of each participant were expressed as an average of stiffness values on each section (in kilopascals, kPa). To discriminate between various METAVIR fibrosis stages at MRE, we used the cutoff values suggested in a previous study (36): 0-2.88 kPa for F0 (no fibrosis), >2.88 kPa for ≥F1 (mild fibrosis), >3.54 kPa for ≥ F2 (significant fibrosis), >3.77 kPa for ≥ F3 (advanced fibrosis), >4.09 kPa for F4 (cirrhosis).

Statistical analysis

Data are expressed as mean ± standard deviation (SD) or number (percentage), as appropriate. Pearson correlation coefficients were calculated to assess the correlation between QUS parameters and MRI-PDFF and LS measurements at SWE and MRE. As the Kolmogorov-Smirnov test rejected the normality of QUS parameters, that of different steatosis grades assessed with MRI-PDFF were compared with the Kruskal-Wallis test. Following this, in the Dunn post-hoc test, a Bonferroni-adjusted P-value less than 0.025 (0.05/2) was considered to indicate statistical significance, as two pairwise comparisons were made between adjacent grades. Receiver operating characteristic (ROC) curve analyses were used to assess the diagnostic performance of QUS parameters and visual steatosis grade for detecting hepatic steatosis (MRI-PDFF ≥5%) and hepatic fat content ≥10% (MRI-PDFF ≥10%). For each ROC analysis, the area under the ROC curve (AUC), optimal cutoff values, and following performance parameters were calculated: sensitivity, specificity, positive predictive value, and negative predictive value. The optimal cutoff value of each QUS parameter was determined using the Youden index (37). Meanwhile, the performance parameters of visual steatosis grade were calculated based on the visual scores (≥S1 [mild] and ≥S2 [moderate], respectively). Pairwise comparisons of AUCs between QUS parameters and visual steatosis grade were performed using the Delong's test. Inter-examination repeatability was evaluated using intra-class correlation coefficients (ICCs) and interpreted as follows: ≥0.90, excellent; 0.75-0.90, good; 0.50-0.75, moderate; and <0.50, poor reliability (38). The coefficient of variation (CV), which is the ratio of the SD to the mean, was also calculated to provide an additional estimate of the reliability,

with the smaller value representing a more reliable measurement (39). Univariate and multivariate linear regression analyses were performed to determine the significant factors affecting QUS parameters. All statistical analyses were performed using MedCalc version 18.11.6 (MedCalc Software, Ostend, Belgium) and SPSS version 25.0 (IBM Corp., Armonk, NY, USA). A P-value of <0.05 was considered statistically significant.

RESULTS

Participant characteristics

A total of 120 participants (75 males and 45 females; mean age, 49.1 years ± 12.6), comprising 96 participants with known or clinically suspected NAFLD and 24 scheduled for liver donation, were included in the analysis. Participant characteristics are summarized in Table 5. Mean MRI-PDFF was 10.2% ± 7.1 (range, 1-37.7%), with 38, 23, and 59 participants with <5%, 5-10%, ≥10% of MRI-PDFF, respectively. Based on the results of MRE, 3.3% (4 of 120) of patients were categorized as having ≥F2. The median interval between US and MRI was 0 days (range, 0-14 days), given that 80.0% of participants (96 of 120) underwent both examinations on the same day.

Correlation between quantitative US parameters and MRI-PDFF

Both AC at TAI and SC at TSI showed significant positive correlations with MRI-PDFF (r= 0.659 and 0.727; 95% confidence interval [CI] = 0.544-0.750 and 0.630-0.802; P<0.001 for both). The distribution of AC at TAI and SC at TSI across the different categories of hepatic fat content assessed with MRI-PDFF is presented in Figure 3 and Table 6. Both AC at TAI and SC at TSI showed significant differences according to hepatic steatosis grades (P<0.001).

Correlations between LS measurements at SWE and MRE

As SWE was defined as showing unreliable results in three patients were defined

as unreliable, correlation between SWE and MRE was assessed in 117 patients with reliable results in both exams. The LS measurements at SWE showed a significant correlation with those with MRE (r=0.793; 95% CI = 0.715-0.852, P<0.001).

Diagnostic performance of quantitative US parameters for hepatic steatosis

The AUCs of AC at TAI and SC at TSI for the detection of hepatic steatosis (MRI-PDFF ≥5%) were 0.861 (95% CI: 0.786-0.918) and 0.964 (95% CI: 0.913-0.989) at the cutoff values of 0.884 dB/cm/MHz and 91.2, respectively. For detecting hepatic steatosis, an AC at TAI >0.884 dB/cm/MHz resulted in a sensitivity of 78.1% (64/82) and specificity of 79.0% (30/38), while an SC at TSI >91.2 resulted in a sensitivity of 85.4% (70/82) and specificity of 97.4% (37/38).

The AUCs of AC at TAI and SC at TSI for the detection of hepatic fat content ≥10% (MRI-PDFF ≥10%) were 0.835 (95% CI: 0.757-0.897) and 0.935 (95% CI: 0.875-0.972) at the cutoff values of 0.980 dB/cm/MHz and 94.0, respectively. The corresponding sensitivity, specificity, positive predictive value, and negative predictive value are shown in Table 7.

For the detection of hepatic steatosis and hepatic fat content ≥10%, SC at TSI showed significantly higher AUCs than the visual steatosis grades of operators (P<0.001 and P=0.026, respectively), while there was no statistically significant difference between the AUCs of AC at TAI and visual steatosis grades operators (P=0.072 and 0.763, respectively). Comparison of diagnostic performance between QUS parameters and visual score of independent reviewer revealed that both AC at

TAI and SC at TSI showed significantly higher AUCs for the detection of hepatic steatosis (P=0.002 and P<0.001, respectively) and hepatic fat content ≥10% (P=0.048 and P<0.001, respectively).

Factors associated with QUS parameters

In univariate linear regression analysis, body mass index (BMI), skin-liver capsule distance, and MRI-PDFF were significant factors affecting AC at TAI. In addition, BMI, skin-liver capsule distance, alanine aminotransferase, and MRI-PDFF significantly affected SC at TSI. On multivariate analysis, MRI-PDFF was an independent determinant for AC at TAI and SC at TSI, showing a positive correlation in both (P<0.001) (Table 8).

Reproducibility of quantitative US parameters

The inter-examination repeatability of SC at TSI was excellent with an ICC of 0.959 (95% CI: 0.941-0.971) and CV of 3.3% (95% CI: 2.9-3.7), and that of AC at TAI was good with an ICC of 0.892 (95% CI: 0.844-0.924) and CV of 6.7% (95% CI: 5.8-7.6).

DISCUSSION

In our study, QUS parameters (AC at TAI and SC at TSI) showed a good correlation with MRI–PDFF (r=0.659 and 0.727; P<0.001 for both) and good diagnostic performance for detecting and grading hepatic steatosis in patients with NAFLD using MRI-PDFF as a standard of reference. Additionally, multivariate linear regression analysis revealed that hepatic fat content assessed by MRI-PDFF was a significant determinant for AC at TAI and SC at TSI. Moreover, their measurements showed good inter-examination repeatability. US beam attenuation increases with depth, which correlates with an increase in AC at TAI (19). Also, as fat droplets act as acoustic scatters in the liver parenchyma, the US backscattered statistics shift from pre-Rayleigh to post-Rayleigh, which increases in SC at TSI (40). This theoretical background could explain the significant positive correlation of both QUS parameters and MRI-PDFF in our study. Considering the significant correlation between QUS parameters and MRI-PDFF obtained in our study and good inter-exam repeatability, QUS parameters could help assess hepatic steatosis as a noninvasive and widely available diagnostic tool.

In our study, both QUS parameters showed good diagnostic performance for detecting hepatic steatosis. AC at TAI provided a sensitivity of 78.1% and specificity of 79.0%, while SC at TSI resulted in a sensitivity of 85.4% and specificity of 97.4%. Moreover, both AC at TAI and SC at TSI provided balanced sensitivity and specificity (sensitivity of 64.4% and 88.1%, and specificity of 93.4% and 86.9%, respectively) for the detection of hepatic fat content ≥10%. These results are consistent with previous studies that showed good diagnostic

performance of US attenuation or backscatter in patients with NAFLD (14, 15). Although MR-based fat quantification is currently accepted as the noninvasive reference standard for the hepatic fat quantification (9, 41), the high cost and limited accessibility of MR is its drawback. We believe that US-based technologies such as QUS could be a promising first-line tool for assessing hepatic steatosis in patients with NAFLD (16). Our results suggest the potential application of AC at TAI and SC at TSI as a screening tool for assessing hepatic steatosis in patients with clinically suspected NAFLD.

In our study, SC at TSI showed significantly better diagnostic performance than visual grade of operator for the detection of MRI-PDFF ≥5% and ≥10%, which was consistent with previous study (42). On the contrary, although the AUCs of AC at TAI were higher than those of visual steatosis grade of operator, there was no statistical significance in our study, while previous study reported better diagnostic performance of AC compared with visual steatosis grade (42). QUS parameters could be useful for the evaluation of hepatic fat contents by providing objective continuous values, while visual assessment provides only subjective categorical values. Application of QUS parameters could be clinically helpful for screening of hepatic steatosis, longitudinal follow-up, and the evaluation of treatment response in patients with hepatic steatosis. In addition, considering the better diagnostic performance of QUS compared with visual grade of less experienced radiologist, QUS could be helpful for less experienced radiologist by providing objective values.

Our study used MRI-PDFF as the reference standard of hepatic steatosis, and we evaluated the diagnostic performance of QUS for detecting MRI-PDFF ≥5% and ≥10%. The reported mean values of MR-PDFF were 3.8%, 12.5%, 16.5% and

26.5% for histologic steatosis grades of S0 (<5%), S1 (5-33%), S2 (33-66%), and S3 (>66%) (31). For discrimination of histologic steatosis grade, reported cutoff values of MRI-PDFF were 4.1-6.4% for discrimination of S0 from S1-3, 15.7-17.4% for S0-1 from S2-3, and 20.9-22.1% for S0-2 from S3 (7, 31, 43). The disparity between MRI-PDFF and histologic fat percentage could be explained by the difference in method for fat quantification. MRI-PDFF estimates the proportion of mobile protons contained within the fat molecules in a three-dimensional liver voxel, whereas histologic analysis evaluates the proportion of hepatocytes which contain macrovesicles of fat in a two-dimensional slide (6, 44, 45). In our study, detecting hepatic steatosis (MRI-PDFF ≥ 5% (14, 32)) was our primary outcome, and detecting hepatic fat content ≥ 10%, defined as MRI-PDFF ≥ 10%, was the secondary outcome of our study as this threshold has been used in several therapeutic clinical trials (14, 33, 46) and hepatic steatosis < 10% is considered as the threshold for living donor liver transplantation to minimize the risk of a graft failure in the recipient and to reduce complication in the donor (47).

In multivariate linear regression analysis, MRI-PDFF was an independent determinant for both AC at TAI and SC at TSI (both P values <0.001). Meanwhile, liver stiffness at MRE, which indicates the degree of hepatic fibrosis, did not show a significant relationship with both AC at TAI and SC at TSI. In previous studies, hepatic fibrosis showed a negative relationship with SC at TSI (reflecting the Nakagami parameter) (42, 48, 49), contrary to our results of the main study. While normal parenchymal tissue showed a near-Rayleigh distribution due to randomly distributed scatterers, the liver parenchymal tissue with fibrotic structures or nodules (resolvable scatterers) tends to demonstrate more of a pre-Rayleigh distribution, resulting in a decrease in the SC at TSI (49). However, liver stiffness

at MRE did not show a significant relationship with SC at TSI in our main study, while liver stiffness showed a significant negative relationship with TSI-p in our pilot study. This difference could be associated with the difference in characteristics of the study population, as the study population of main study had only a small percentage of patients with significant fibrosis (11.7%, 14/120), there could be a limitation in evaluating the relationship between QUS parameters and hepatic fibrosis. However, as the hepatic fibrosis of pilot study was also assessed only using TE, without histologic results, further study using histologic reference standard to validate the association between hepatic fibrosis and SC at TSI are warranted.

Meanwhile, there are some controversies regarding the relationship between hepatic fibrosis and AC at TAI (US attenuation); a previous study suggested that hepatic fibrosis showed a positive correlation with US attenuation (50), while another study showed no significant relationship (51), which was consistent with our study result. Theoretically, the attenuation of the US beam could be affected by fibrosis, although it is less than that by steatosis (52). The results of AC at TAI was also explained by the study population deviation, with only a small percentage with significant fibrosis according to MRE stiffness values. Further study with large population having various fibrosis stages could help in the precise evaluation of the relationship between hepatic fibrosis and QUS parameters.

Our study has several limitations. First, the study population was biased toward NAFLD, as only 31.7% of patients were normal (MRI-PDFF<5%), which is different from the prevalence in the general population. Second, although the QUS technique from RF data analysis can be implemented into the clinical US systems, this technique is not readily available in all clinical US systems. However, with

most manufacturers beginning to provide RF output capabilities, it could be widely available in the near future. Third, Effect of other histologic features of NAFLD, such as inflammation or fibrosis, on QUS parameters were not validated. Although we performed a subgroup analysis of patients with histopathologic reference standard (Appendix 2), the results needs to be further validated as only living donor for liver transplantation were included. Further validation study with histologic reference would be needed.

In conclusion, AC at TAI and SC at TSI derived from quantitative US RF data analysis yielded a good correlation with MRI-PDFF and provided good performance for detecting hepatic steatosis and assessing its severity in NAFLD.

REFERENCES

1. Castera L, Friedrich-Rust M, Loomba R. Noninvasive Assessment of Liver Disease in Patients With Nonalcoholic Fatty Liver Disease. Gastroenterology. 2019;156(5):1264-81.e4.
2. Vernon G, Baranova A, Younossi ZM. Systematic review: the epidemiology and natural history of non-alcoholic fatty liver disease and non-alcoholic steatohepatitis in adults. Aliment Pharmacol Ther. 2011;34(3):274-85.
3. Friedman SL, Neuschwander-Tetri BA, Rinella M, Sanyal AJ. Mechanisms of NAFLD development and therapeutic strategies. Nature medicine. 2018;24(7):908-22.
4. Pais R, Barritt ASt, Calmus Y, et al. NAFLD and liver transplantation: Current burden and expected challenges. J Hepatol. 2016;65(6):1245-57.
5. Machado MV, Cortez-Pinto H. Non-invasive diagnosis of non-alcoholic fatty liver disease. A critical appraisal. J Hepatol. 2013;58(5):1007-19.
6. Reeder SB, Cruite I, Hamilton G, Sirlin CB. Quantitative Assessment of Liver Fat with Magnetic Resonance Imaging and Spectroscopy. J Magn Reson Imaging. 2011;34(4):729-49.
7. Tang A, Desai A, Hamilton G, et al. Accuracy of MR imaging-estimated proton density fat fraction for classification of dichotomized histologic steatosis grades in nonalcoholic fatty liver disease. Radiology. 2015;274(2):416-25.
8. Yokoo T, Serai SD, Pirasteh A, et al. Linearity, Bias, and Precision of Hepatic Proton Density Fat Fraction Measurements by Using MR Imaging: A Meta-Analysis. Radiology. 2018;286(2):486-98.
9. Kramer H, Pickhardt PJ, Kliewer MA, et al. Accuracy of Liver Fat Quantification With Advanced CT, MRI, and Ultrasound Techniques: Prospective Comparison With MR Spectroscopy. AJR Am J Roentgenol. 2017;208(1):92-100.
10. Zhou Z, Zhang Q, Wu W, et al. Hepatic steatosis assessment using ultrasound homodyned-K parametric imaging: the effects of estimators. Quant Imaging Med Surg. 2019;9(12):1932-47.
11. Dasarathy S, Dasarathy J, Khiyami A, Joseph R, Lopez R, McCullough AJ. Validity of real time ultrasound in the diagnosis of hepatic steatosis: a prospective study. J Hepatol. 2009;51(6):1061-7.
12. Eddowes PJ, Sasso M, Allison M, et al. Accuracy of FibroScan Controlled Attenuation Parameter and Liver Stiffness Measurement in Assessing Steatosis and Fibrosis in Patients With Nonalcoholic Fatty Liver Disease. Gastroenterology. 2019;156(6):1717-30.
13. Nam K, Rosado-Mendez IM, Wirtzfeld LA, et al. Comparison of ultrasound attenuation and backscatter estimates in layered tissue-mimicking phantoms among three clinical scanners. Ultrasonic imaging.

2012;34(4):209-21.
14. Lin SC, Heba E, Wolfson T, et al. Noninvasive Diagnosis of Nonalcoholic Fatty Liver Disease and Quantification of Liver Fat Using a New Quantitative Ultrasound Technique. Clin Gastroenterol Hepatol. 2015;13(7):1337-45.e6.
15. Paige JS, Bernstein GS, Heba E, et al. A Pilot Comparative Study of Quantitative Ultrasound, Conventional Ultrasound, and MRI for Predicting Histology-Determined Steatosis Grade in Adult Nonalcoholic Fatty Liver Disease. AJR Am J Roentgenol. 2017;208(5):W168-w77.
16. Yang KC, Liao YY, Tsui PH, Yeh CK. Ultrasound imaging in nonalcoholic liver disease: current applications and future developments. Quant Imaging Med Surg. 2019;9(4):546-51.
17. Joo I, Kim SY, Park HS, Lee ES, Kang HJ, Lee JM. Validation of a New Point Shear-Wave Elastography Method for Noninvasive Assessment of Liver Fibrosis: A Prospective Multicenter Study. Korean J Radiol. 2019;20(11):1527-35.
18. Hamaguchi M, Kojima T, Itoh Y, et al. The severity of ultrasonographic findings in nonalcoholic fatty liver disease reflects the metabolic syndrome and visceral fat accumulation. Am J Gastroenterol. 2007;102(12):2708-15.
19. Kim H, Varghese T. Attenuation estimation using spectral cross-correlation. IEEE Trans Ultrason Ferroelectr Freq Control. 2007;54(3):510-9.
20. Tsui PH, Wan YL, Tai DI, Shu YC. Effects of Estimators on Ultrasound Nakagami Imaging in Visualizing the Change in the Backscattered Statistics from a Rayleigh Distribution to a Pre-Rayleigh Distribution. Ultrasound Med Biol. 2015;41(8):2240-51.
21. Liao YY, Yang KC, Lee MJ, Huang KC, Chen JD, Yeh CK. Multifeature analysis of an ultrasound quantitative diagnostic index for classifying nonalcoholic fatty liver disease. Sci Rep. 2016;6:35083.
22. Chon YE, Jung KS, Kim SU, et al. Controlled attenuation parameter (CAP) for detection of hepatic steatosis in patients with chronic liver diseases: a prospective study of a native Korean population. Liver international : official journal of the International Association for the Study of the Liver. 2014;34(1):102-9.
23. Wong VW, Petta S, Hiriart JB, et al. Validity criteria for the diagnosis of fatty liver by M probe-based controlled attenuation parameter. J Hepatol. 2017;67(3):577-84.
24. Castera L, Forns X, Alberti A. Non-invasive evaluation of liver fibrosis using transient elastography. J Hepatol. 2008;48(5):835-47.
25. Castéra L, Vergniol J, Foucher J, et al. Prospective comparison of transient elastography, Fibrotest, APRI, and liver biopsy for the assessment of fibrosis in chronic hepatitis C. Gastroenterology. 2005;128(2):343-50.
26. Kobus T, van der Laak JA, Maas MC, et al. Contribution of histopathologic tissue composition to quantitative MR spectroscopy and diffusion-weighted imaging of the prostate. Radiology. 2016;278(3):801-11.
27. Dietrich CF, Bamber J, Berzigotti A, et al. EFSUMB Guidelines and

Recommendations on the Clinical Use of Liver Ultrasound Elastography, Update 2017 (Long Version). Ultraschall in der Medizin (Stuttgart, Germany : 1980). 2017;38(4):e16-e47.
28. Choi K, Kong D, Hah Z, Lee H-K. A reliability index of shear wave speed measurement for shear wave elastography. 2015 IEEE international ultrasonics symposium (IUS): IEEE, 2015; p. 1-4.
29. Reeder SB, Robson PM, Yu H, et al. Quantification of hepatic steatosis with MRI: the effects of accurate fat spectral modeling. J Magn Reson Imaging. 2009;29(6):1332-9.
30. Hamilton G, Yokoo T, Bydder M, et al. In vivo characterization of the liver fat ^{1}H MR spectrum. NMR Biomed. 2011;24(7):784-90.
31. Tang A, Tan J, Sun M, et al. Nonalcoholic fatty liver disease: MR imaging of liver proton density fat fraction to assess hepatic steatosis. Radiology. 2013;267(2):422-31.
32. Han A, Zhang YN, Boehringer AS, et al. Assessment of Hepatic Steatosis in Nonalcoholic Fatty Liver Disease by Using Quantitative US. Radiology. 2020;295(1):106-13.
33. Caussy C, Alquiraish MH, Nguyen P, et al. Optimal threshold of controlled attenuation parameter with MRI-PDFF as the gold standard for the detection of hepatic steatosis. Hepatology (Baltimore, Md). 2018;67(4):1348-59.
34. Lee DH, Lee JM, Yi NJ, et al. Hepatic stiffness measurement by using MR elastography: prognostic values after hepatic resection for hepatocellular carcinoma. Eur Radiol. 2017;27(4):1713-21.
35. Yoon JH, Lee JM, Woo HS, et al. Staging of hepatic fibrosis: comparison of magnetic resonance elastography and shear wave elastography in the same individuals. Korean J Radiol. 2013;14(2):202-12.
36. Singh S, Venkatesh SK, Loomba R, et al. Magnetic resonance elastography for staging liver fibrosis in non-alcoholic fatty liver disease: a diagnostic accuracy systematic review and individual participant data pooled analysis. Eur Radiol. 2016;26(5):1431-40.
37. Youden WJ. Index for rating diagnostic tests. Cancer. 1950;3(1):32-5.
38. Koo TK, Li MY. A Guideline of Selecting and Reporting Intraclass Correlation Coefficients for Reliability Research. J Chiropr Med. 2016;15(2):155-63.
39. Bland JM, Altman DG. Statistical methods for assessing agreement between two methods of clinical measurement. Lancet. 1986;1(8476):307-10.
40. Wan YL, Tai DI, Ma HY, Chiang BH, Chen CK, Tsui PH. Effects of fatty infiltration in human livers on the backscattered statistics of ultrasound imaging. Proc Inst Mech Eng H. 2015;229(6):419-28.
41. Gu J, Liu S, Du S, et al. Diagnostic value of MRI-PDFF for hepatic steatosis in patients with non-alcoholic fatty liver disease: a meta-analysis. Eur Radiol. 2019;29(7):3564-73.
42. Jeon SK, Joo I, Kim SY, et al. Quantitative ultrasound radiofrequency data analysis for the assessment of hepatic steatosis using

the controlled attenuation parameter as a reference standard. Ultrasonography. 2020.
43. Runge JH, Smits LP, Verheij J, et al. MR Spectroscopy-derived Proton Density Fat Fraction Is Superior to Controlled Attenuation Parameter for Detecting and Grading Hepatic Steatosis. Radiology. 2018;286(2):547-56.
44. Kleiner DE, Brunt EM, Van Natta M, et al. Design and validation of a histological scoring system for nonalcoholic fatty liver disease. Hepatology (Baltimore, Md). 2005;41(6):1313-21.
45. Brunt EM, Janney CG, Di Bisceglie AM, Neuschwander-Tetri BA, Bacon BR. Nonalcoholic steatohepatitis: a proposal for grading and staging the histological lesions. Am J Gastroenterol. 1999;94(9):2467-74.
46. Sumida Y, Yoneda M. Current and future pharmacological therapies for NAFLD/NASH. Journal of gastroenterology. 2018;53(3):362-76.
47. Rinella ME, Alonso E, Rao S, et al. Body mass index as a predictor of hepatic steatosis in living liver donors. Liver transplantation : official publication of the American Association for the Study of Liver Diseases and the International Liver Transplantation Society. 2001;7(5):409-14.
48. Tsui PH, Ho MC, Tai DI, Lin YH, Wang CY, Ma HY. Acoustic structure quantification by using ultrasound Nakagami imaging for assessing liver fibrosis. Sci Rep. 2016;6:33075.
49. Yamada H, Ebara M, Yamaguchi T, et al. A pilot approach for quantitative assessment of liver fibrosis using ultrasound: preliminary results in 79 cases. J Hepatol. 2006;44(1):68-75.
50. Jeon SK, Lee JM, Joo I, et al. Prospective Evaluation of Hepatic Steatosis Using Ultrasound Attenuation Imaging in Patients with Chronic Liver Disease with Magnetic Resonance Imaging Proton Density Fat Fraction as the Reference Standard. Ultrasound Med Biol. 2019;45(6):1407-16.
51. Tada T, Kumada T, Toyoda H, et al. Liver stiffness does not affect ultrasound-guided attenuation coefficient measurement in the evaluation of hepatic steatosis. Hepatol Res. 2020;50(2):190-8.
52. Lin T, Ophir J, Potter G. Correlation of ultrasonic attenuation with pathologic fat and fibrosis in liver disease. Ultrasound Med Biol. 1988;14(8):729-34.
53. Kim H, Varghese T. Attenuation estimation using spectral cross-correlation. ieee transactions on ultrasonics, ferroelectrics, and frequency control. 2007;54(3):510-9.
54. Liao Y-Y, Yang K-C, Lee M-J, Huang K-C, Chen J-D, Yeh C-K. Multifeature analysis of an ultrasound quantitative diagnostic index for classifying nonalcoholic fatty liver disease. Scientific reports. 2016;6:35083.
55. Shankar PM. A general statistical model for ultrasonic backscattering from tissues. IEEE transactions on ultrasonics, ferroelectrics, and frequency control. 2000;47(3):727-36.
56. Ho M-C, Lee Y-H, Jeng Y-M, Chen C-N, Chang K-J, Tsui P-H. Relationship between ultrasound backscattered statistics and the concentration of fatty droplets in livers: an animal study. PLoS One. 2013;8(5).

57. Tsui P-H, Wan Y-L. Application of ultrasound nakagami imaging for the diagnosis of fatty liver. Journal of Medical Ultrasound. 2016;24(2):47-9.
58. Bedossa P, Poynard T. An algorithm for the grading of activity in chronic hepatitis C. The METAVIR Cooperative Study Group. Hepatology (Baltimore, Md). 1996;24(2):289-93.
59. Park YN, Chon CY, Park JB, et al. Histological grading and staging of chronic hepatitis standardized guideline proposed by the Korean Study Group for the Pathology of Digestive Diseases. 1999;33(5):337-46.

Table 1. Patient characteristics of the pilot study

Characteristics	Patients (n=243)
Age (years), mean ± SD (range)	55 ± 13 (18-83)
Sex (Male: Female)	171:72
Body mass index (kg/m^2), mean ± SD (range)	25 ± 4 (17-31)
Skin-liver capsule distance (mm), mean ± SD (range)	18 ± 4 (10-36)
Etiology of chronic liver disease	
Chronic hepatitis B	116 (47.7)
Chronic hepatitis C	41 (16.9)
Alcoholic liver disease	10 (4.1)
Unknown or other causes	34 (14.0)
No underlying liver disease	42 (17.3)
Aspartate aminotransferase (IU/L), mean ± SD (range)	30 ± 17 (10-161)
Alanine aminotransferase (IU/L), mean ± SD (range)	30 ± 18 (5-117)
Hepatic fibrosis grades	
F0 or F1 (≤7.1 kPa on TE)	145 (59.7)
F2 (>7.1 to ≤9.5 kPa on TE)	31 (12.8)
F3 (>9.5 to ≤12.5 kPa on TE)	25 (10.3)
F4 (>12.5 kPa on TE)	42 (17.3)
Hepatic steatosis grades	
S0 (≤250 dB/m on CAP)	152 (62.6)
S1 (>250 to ≤299 dB/m on CAP)	54 (22.2)
S2 (>299 to ≤327 dB/m on CAP)	14 (5.8)
S3 (>327 dB/m on CAP)	23 (9.5)

Note. Data are percentages (numbers used to calculate percentages), unless otherwise specified. SD = standard deviation, TE = transient elastography, CAP = controlled attenuation parameter.

Table 2. Diagnostic performance of US parameters in the prediction of hepatic steatosis grades

US parameters	Hepatic steatosis grades	AUC (95% CI)	Cut-off	Sensitivity (%)	Specificity (%)
Visual score (0-3)	≥S1	0.659 (0.596, 0.719)	≥Score 1 (mild)	63.7 (58/91)	56.6 (86/152)
	≥S2	0.778 (0.721, 0.829)	≥Score 2 (moderate)	51.4 (19/37)	96.1 (198/206)
	S3	0.794 (0.737, 0.843)	Score 3 (severe)	8.7 (2/23)	100 (220/220)
TAI-p (MHz/cm)	≥S1	0.844 (0.793, 0.888)	≤-0.078	83.5 (76/91)	77.6 (118/152)
	≥S2	0.914 (0.872, 0.946).	≤-0.093	91.9 (34/37)	84.0 (173/206)
	S3	0.909 (0.866, 0.942)	≤-0.093	95.7 (22/23)	79.6 (175/220)
TSI-p	≥S1	0.827 (0.773, 0.872)	>0.910	65.9 (60/91)	92.8 (141/152)
	≥S2	0.914 (0.871, 0.946)	>0.952	86.5 (32/37)	86.9 (179/206)
	S3	0.917 (0.875, 0.948)	>0.952	95.7 (22/23)	83.2 (183/220)

Note. Data in sensitivity and specificity are percentages (numbers used to calculate percentages). AUC = area under the receiver operating characteristics (ROC) curve, CI = confidence interval, TAI-p=tissue attenuation imaging parameter, TSI-p=tissue scatter-distribution imaging parameter, US = ultrasound.

Table 3. Comparison of diagnostic performance of ultrasound parameters for the assessment of hepatic steatosis grade

Hepatic steatosis grades	AUC (95% CI)‡			P value for pairwise comparison of AUCs		
	i) Visual score	ii) TAI-p	iii) TSI-p	i) versus ii)	i) versus iii)	ii) versus iii)
≥S1	0.659 (0.596, 0.719)	0.844 (0.793, 0.888)	0.827 (0.773, 0.872)	<0.001*	<0.001*	0.705
≥S2	0.778 (0.721, 0.829)	0.914 (0.872, 0.946).	0.914 (0.871, 0.946)	0.003*	<0.001*	0.985
S3	0.794 (0.737, 0.843)	0.909 (0.866, 0.942)	0.917 (0.875, 0.948)	0.029	0.006*	0.750

Note. AUC = area under the receiver operating characteristics (ROC) curve, CI = confidence interval, TAI-p = tissue attenuation imaging parameter, TSI-p = tissue scatter-distribution imaging parameter. *P values indicate those are statistically significant (<0.017 [0.05/3, according to Bonferroni-correction]).

Table 4. Univariate and multivariate linear regression analysis for identifying determinants for US radiofrequency data-driven parameters

Parameters	Univariate linear regression analysis		Multivariate linear regression analysis	
	Coefficient (95% CI) ($\times 10^{-3}$)	P value	Coefficient (95% CI) ($\times 10^{-3}$)	P value
TAI-p (MHz/cm)				
Gender (Male 0, Female 1)	1 (-9, 12)	0.791		
Age (years)	0.1 (-0.2, 0.5)	0.536		
Body mass index (kg/m^2)	-3 (-4, -2)	<0.001*	1 (-0.6, 2.5)	0.216
Skin-liver capsule distance (mm)	-3 (-4, -2)	<0.001*	-0.9 (-1.9, 0.2)	0.098
Aspartate aminotransferase (IU/L)	-0.1 (-0.4, 0.1)	0.292		
Alanine aminotransferase (IU/L)	-0.3 (-0.6, -0.1)	0.020*	-0.1 (-0.3, 0.2)	0.662
Hepatic fibrosis grades based on TE†	-2 (-6, 2)	0.259		
Hepatic steatosis grades based on CAP‡	-24 (-27, -20)	<0.001*	-22 (-26, -18)	<0.001*
TSI-p				
Gender (Male: 0, Female: 1)	30 (-4, 64)	0.085		
Age (years)	-0.7 (-1.9, 0.5)	0.247		
Body mass index (kg/m^2)	9 (2, 15)	0.012*	8 (-1, 15)	0.057
Skin-liver capsule distance (mm)	-2 (-7, 4)	0.588		
Aspartate aminotransferase (IU/L)	0.9 (-0.5, 2.3)	0.192		
Alanine aminotransferase (IU/L)	0.4 (-0.9, 1.6)	0.549		
Hepatic fibrosis grades based on TE†	-18 (-33, -4)	0.015*	-14 (-27, -1)	0.034*
Hepatic steatosis grades based on CAP‡	83 (65, 101)	<0.001*	84 (67, 102)	<0.001*

Note. *P values indicate those are statistically significant. †Assigned as F0/1, 1; F2, 2; F3, 3; and F4, 4. ‡Assigned as S0, 0; S1, 1; S2, 2; and S3, 3. US = ultrasound, CI = confidence interval, TE = transient elastography, CAP = controlled attenuation parameter.

Table 5. Patient characteristics of the main study

Variable	Value (n=120)
Age (years)	49.1 ± 12.6 (20-73)
Sex	
Male	75 (62.5)
Female	45 (37.5)
BMI (kg/m^2)	26.1 ± 3.5 (18.1-37.2)
Skin-to-liver capsule distance (mm)	19.2 ± 3.9 (11-36)
Aspartate aminotransferase (IU/L)	37.3 ± 34.6 (12-258)
Alanine aminotransferase (IU/L)	45.5 ± 42.0 (9-313)
Hepatic fibrosis grades	
<F2 (without significant fibrosis)	106 (88.3)
≥F2 (with significant fibrosis)	14 (11.7)
Visual hepatic steatosis grade	
S0	49 (40.8)
S1	28 (23.3)
S2	30 (25.0)
S3	13 (10.8)
MRI-PDFF (%)	10.2 ± 7.1 (1-37.7)
<5%	38 (31.7)
≥5 to <10%	23 (19.2)
≥10%	59 (49.2)

Note. Values are presented as mean ± standard deviation (range) or number (%) as appropriate. BMI = body mass index, MRI-PDFF = magnetic resonance imaging proton density fat fraction.

Table 6. Quantitative US parameters according to hepatic steatosis grades

Quantitative US parameters	Hepatic steatosis grade			P value		
	MRI-PDFF <5% (n=38)	MRI-PDFF 5-10% (n=23)	MRI-PDFF ≥10% (n=59)	Kruskal-Wallis test	Dunn's post hoc test	
					<5% vs. 5-10%	5-10% vs. ≥10%
AC at TAI (dB/cm/MHz)	0.829 ± 0.085	0.915 ± 0.063	1.006 ± 0.119	<0.001	0.013	0.015
SC at TSI	80.3 ± 7.3	91.9 ± 5.5	98.7 ± 4.7	<0.001	0.001	0.001

Note. Values are presented as mean ± standard deviation unless otherwise specified. US = ultrasound, AC = attenuation coefficient, TAI = tissue attenuation imaging, SC = scatter-distribution coefficient, TSI = tissue scatter-distribution imaging, MRI-PDFF = magnetic resonance imaging proton density fat fraction.

Table 7. Diagnostic performance of quantitative US parameters and visual grade for the detection of hepatic steatosis

US parameters	Hepatic fat content	AUC (95% CI)	Cut-off value	Sensitivity (%)	Specificity (%)	PPV (%)	NPV (%)
Quantitative US parameters							
AC at TAI (dB/cm/MHz)							
	MRI-PDFF ≥5%	0.861 (0.786, 0.918)	>0.884	78.1 (64/82)	79.0 (30/38)	88.9 (64/72)	62.5 (30/48)
	MRI-PDFF ≥10%	0.835 (0.757, 0.897)	>0.980	64.4 (38/59)	93.4 (57/61)	90.5 (38/42)	73.1 (57/78)
SC at TSI							
	MRI-PDFF ≥5%	0.964 (0.913, 0.989)	>91.2	85.4 (70/82)	97.4 (37/38)	98.6 (70/71)	75.5 (37/49)
	MRI-PDFF ≥10%	0.935 (0.875, 0.972)	>94.0	88.1 (52/59)	86.9 (53/61)	86.7 (52/60)	88.3 (53/60)
Visual steatosis grade							
Operator	MRI-PDFF ≥5%	0.779 (0.694, 0.850)	≥S1 (mild)	76.8 (63/82)	79.0 (30/38)	88.7 (63/71)	61.2 (30/49)
	MRI-PDFF ≥10%	0.848 (0.771, 0.907)	≥S2 (moderate)	71.2 (42/59)	98.4 (60/61)	97.7 (42/43)	77.9 (60/77)
Independent reviewer							
	MRI-PDFF ≥5%	0.730 (0.641, 0.807)	≥S1 (mild)	81.7 (67/82)	36.8 (14/38)	73.6 (67/91)	48.3 (14/29)
	MRI-PDFF ≥10%	0.753 (0.666, 0.827)	≥S2 (moderate)	57.6 (34/59)	86.9 (53/61)	81.0 (34/42)	67.9 (53/78)

Note. US = ultrasound, AUC = area under the receiver operating characteristic curve, PPV = positive predictive value, NPV = negative predictive value, AC = attenuation coefficient, TAI = tissue attenuation imaging, SC = scatter-distribution coefficient, TSI = tissue scatter-distribution imaging, MRI-PDFF = magnetic resonance imaging proton density fat fraction.

Table 8. Univariate and multivariate linear regression analysis for analyzing factors associated with quantitative US parameters

Parameter	Univariate analysis		Multivariate analysis	
	Coefficient (95% CI) ($x10^{-3}$)	P value	Coefficient (95% CI) ($x10^{-3}$)	P value
AC at TAI (dB/cm/MHz)				
Female gender	-2 (-49, 46)	0.941		
Age (yr)	1 (-0.1, 3)	0.152		
BMI (kg/m^2)	13 (7, 19)	**<0.001**	0.1 (-7. 7)	0.944
Skin-liver capsule distance (mm)	10 (4, 15)	**0.001**	3 (-1, 8)	0.146
Aspartate aminotransferase (IU/L)	-0.9 (-1, 1)	0.782		
Alanine aminotransferase (IU/L)	0.5 (-0.1, 1)	0.125		
MRI-PDFF (%)	12 (9, 14)	**<0.001**	12 (8, 14)	**<0.001**
LS at MRE (kPa)	23 (-9, 55)	0.150		
SC at TSI				
Female gender	-42 (-78, 5)	0.250		
Age (yr)	2 (-1, 3)	0.132		
BMI (kg/m^2)	13 (9, 18)	**<0.001**	5 (-0.3, 10)	0.072
Skin-liver capsule distance (mm)	8 (4, 12)	**<0.001**	1 (-0.4, 5)	0.858
Aspartate aminotransferase (IU/L)	0.3 (-0.2, 1)	0.300		
Alanine aminotransferase (IU/L)	0.6 (0.1, 1)	**0.007**	0.1 (-0.3, 0.6)	0.924
MRI-PDFF (%)	10 (8, 12)	**<0.001**	9 (7, 11)	**<0.001**
LS at MRE (kPa)	22 (-3, 47)	0.080		

Note. 95% CI= 95% confidence interval, AC = attenuation coefficient, TAI = tissue attenuation imaging, BMI = body mass index, MRI-PDFF = magnetic resonance imaging proton density fat fraction, LS = liver stiffness, MRE = magnetic resonance elastography, SC = scatter-distribution coefficient, TSI = tissue scatter-distribution imaging.

Figure 1. Flowchart of the study population. MRI-PDFF = magnetic resonance imaging -proton density fat fraction.

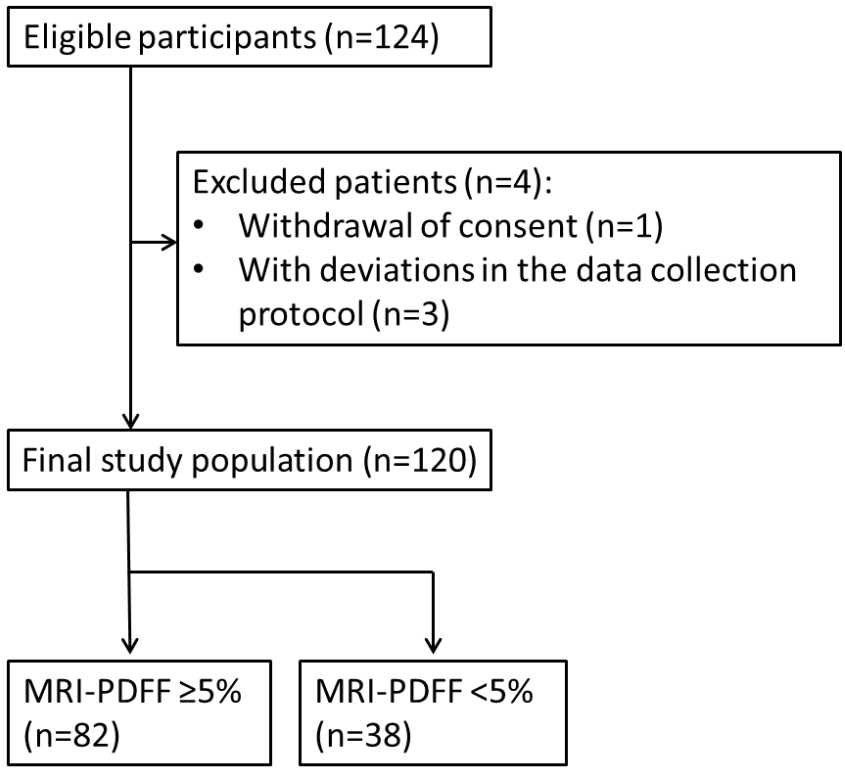

Figure 2. Quantitative ultrasound parameters of radiofrequency data analysis. From acquired radiofrequency data of B-mode ultrasound image (a), color-coded maps of tissue attenuation imaging (TAI) map reflecting center frequency (b), and tissue scatter-distribution imaging (TSI) map reflecting Nakagami parameters (c) are generated. With reference to the B-mode image, the annulus-sector region of interests (ROIs) are drawn in TAI map (b) and TSI map (c), respectively. The attenuation coefficient (AC) at TAI and the scatter-distribution coefficient (SC) at TSI are obtained.

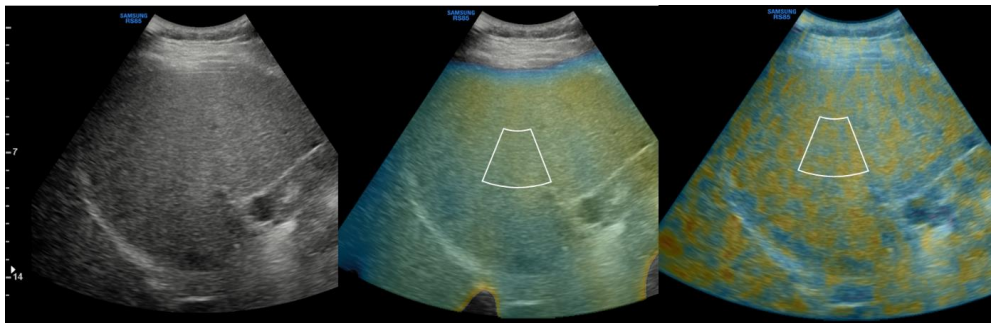

Figure 3. The distribution of quantitative ultrasound parameters according to hepatic fat content at magnetic resonance imaging proton density fat fraction (MRI-PDFF). The distribution of attenuation coefficient at tissue attenuation imaging (AC at TAI, a) and scatter-distribution coefficient at tissue scatter-distribution imaging (SC at TSI, b) is stratified by hepatic fat content at MRI-PDFF. Asterisk (*) indicates statistical significance.

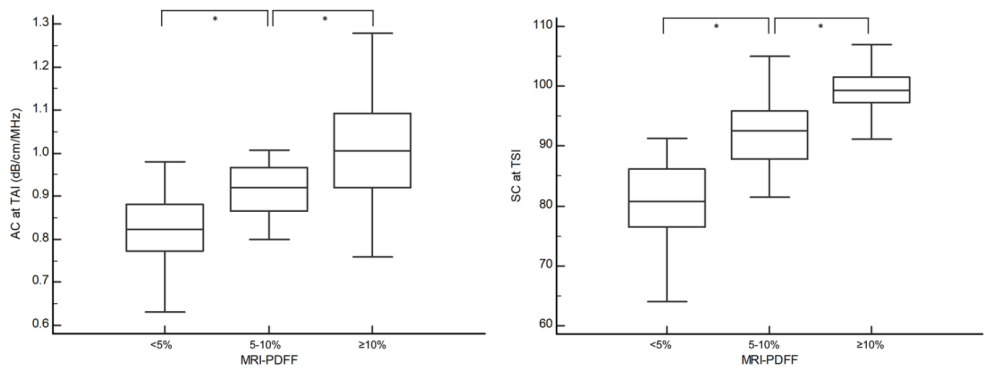

APPENDIX

Appendix 1. Quantitative ultrasound parameters from radiofrequency data analysis: theoretical background and how to create parametric maps

Tissue attenuation imaging (TAI)

Tissue attenuation imaging (TAI) is based on the ultrasound attenuation properties of different frequency components in the tissue. As the attenuation of higher frequency components is greater than that of lower frequency components, the power spectrum of radiofrequency signals by using short-time Fourier analysis demonstrates a downward shift of the center frequency along with the depth. Assuming a Gaussian-shaped transmit pulse with invariant variance along with the depth, the relationship between the center frequency shift and attenuation coefficient (AC, β) is given by as following (53, 54): $\beta\ (dB/cm/MHz) = -\frac{8.686}{4\sigma^2} \cdot \frac{df_c(z)}{dz}$ "", where z is the depth of the region of interest from the transducer, σ^2 is the variance of the transmit pulse, and fc(z) is the center frequency of the power spectrum at depth z. Tissue attenuation imaging parameter (TAI-p) is calculated based on the frequency shift along with the depth which linearly correlates the attenuation coefficient as follows: TAI-p $= \frac{df_c(z)}{dz}$. The Fourier transform is used to calculate the block power spectrum, and the estimated center frequency is defined as the average frequency in the block power spectrum.

To create a TAI map comprising local center frequency, the sliding window (3 mm x 1 scan-line) technique is applied through the entire radiofrequency signal

data with a shift of one-pixel step, and the local center frequency is assigned to a new pixel located at the center of the window each time.

Tissue scatter-distribution imaging (TSI)

Tissue scatter-distribution imaging (TSI) a pixel-by-pixel map of the Nakagami parameter, which is the shape parameter of the Nakagami distribution. It depends on the arrangements and concentration of the scatterers (55-57).

The Nakagami parameter can be calculated as follows: "$Nakagami\ parameter = \frac{[E(R^2)]^2}{E[R^4]-[E(R^2)]^2}$", where R and E(·) represents the backscattered-signal envelope and the expected value, respectively. The Nakagami parameter varied from 0 to 1 when the statistics of the backscattered-signal envelope changed from pre-Rayleigh to Rayleigh distribution. Pre-Rayleigh indicates there are a small number of scatterers randomly distributed in the ultrasound resolution cell, while Rayleigh distribution indicates the high density of randomly distributed scatterers without coherent signal components. When the Nakagami parameter is larger than 1, the backscattered-signal statistics correspond to post-Rayleigh distribution, meaning there are periodic scatterers or local high-concentration scatterer aggregation, in addition to many scatterers randomly distributed in the resolution cell.

To construct a TSI map comprising local Nakagami parameters, the square sliding window (3×3 mm^2) technique is applied through the entire envelope image with the shift of one-pixel step, which assigns a local Nakagami parameter for a new pixel located at the center of the window each time.

Appendix 2. Subgroup analysis in patients with histopathologic reference standard

For 24 patients with available specimens for histopathologic analysis of hepatic steatosis, pathologic results were reviewed. The degree of hepatic steatosis was determined according to the histological scoring system for NAFLD as follows: S0 (< 5%, none); S1 (5–33%, mild); S2 (> 33–66%, moderate); and S3 (> 66%, severe) (44). Fibrosis and necroinflammatory activity in the liver were also evaluated by the standardized guidelines established by the Korean Study Group for the Pathology of Digestive Diseases, which is similar to the METAVIR scoring system (58, 59). Fibrosis was graded on a 0–4 scale as follows: F0 (no fibrosis), F1 (portal fibrosis without septa), F2 (portal fibrosis and few septa), F3 (numerous septa without cirrhosis), and F4 (cirrhosis). The necroinflammatory activity consisted of lobular activity and porto-periportal activity, and both were graded using a 4-point scale as follows: score 0 (none), score 1 (minimal), score 2 (mild), score 3 (moderate), and score 4 (severe).

In our study, patients who are available specimens for histopathologic analysis were patients who underwent hepatectomy for liver donation. 21 patients were defined as S0 and 3 patients were defined as S1. Regarding the fibrosis, 20 patients were classified as F0 and 5 patients were as F1. Regarding the necroinflammatory activity, 20 patients were in score 0, 3 patients were in score 1, and 1 patients in score 2, respectively.

AC at TAI didn’t show significant difference between S0 and S1 groups (0.800 ± 0.053 vs. 0.910 ± 0.113. P=0.106). SC at TSI didn’t show significant difference between S0 and S1 (81.0 ± 9.4 vs. 82.4 ± 6.0, P=0.805).

초 록

비알코올성 지방간 환자에서 정량적 초음파 영상 지표의 개발 및 지방간 진단능 평가

배경 및 목적: 본 연구에서는 비알코올성 지방간 환자에서 지방간 정도를 평가하기 위한 정량적 초음파 지표를 개발하고, 자기공명영상 양성자밀도 지방분율을 기준으로 하여 정량적 초음파 지표의 지방간 진단능을 평가하고자 한다.

재료 및 방법: 본 단일센터 전향적 연구에서는 2019년 3월부터 2020년 1월까지 임상적으로 비알코올성 지방간이 의심되는 환자와 간이식 공여자를 포함한 총 120명의 참가자가 등록되었다. 참가자들은 무선주파수 (radiofrequency, RF) 데이터를 얻기 위한 초음파 검사와 자기공명영상 양성자밀도 지방분율(Magnetic resonance imaging proton density fat fraction, MRI-PDFF) 검사를 시행하였다. 초음파 RF 데이터를 분석하여, 조직감쇠영상(tissue attenuation imaging, TAI)에서의 감쇠계수 (attenuation coefficient, AC)와 조직 산란분포 영상(tissue scatter-distribution imaging, TSI)에서의 산란분포계수 (scatter-distribution coefficient, SC)를 획득하였다. 이 두 정량적 초음파 지표 (AC, SC)와 자기공명영상 양성자밀도 지방분율(MRI-PDFF) 사이의 연관성을 피어슨 상관계수를 통해 분석하였다. 정량적 초음파 지표들이 MRI-PDFF ≥5% 와 MRI-PDFF

≥10%의 지방간을 진단하는 진단능을 Receiver operating characteristics (ROC) 분석을 통해 확인하였다. 또한, 다변량 회귀분석(multivariate linear regression analysis)을 통해, 두 정량적 초음파 지표에 영향을 주는 임상 또는 영상적 지표를 확인하였다.

결과: 참가자는 지방간 정도에 따라 세 단계로 구분되었다 (MRI-PDFF <5% (n=38), 5-10% (n=23), and ≥10% (n=59)). 감쇠계수 (AC at TAI)와 산란분포계수 (SC at TSI)는 자기공명영상 양성자밀도 지방분율과 강한 상관관계를 보였다 (r=0.659 and 0.727, P<0.001 for both). 지방간 유무 진단 (MRI-PDFF ≥5%)과 MRI-PDFF ≥10%의 지방간진단에 있어 감쇠계수의 진단능은 0.861 (95% confidence interval [CI]: 0.786-0.918) 과 0.835 (95% CI: 0.757-0.897)이었고, 산란분포계수의 진단능은 0.964 (95% CI: 0.913-0.989) and 0.935 (95% CI: 0.875-0.972) 이었다. 다변량회귀분석에서 지방분율이 정량적 초음파 지표와 연관성을 보이는 유일한 독립적인 인자로 확인되었다.

결론: 본 연구에서 감쇠계수 (AC at TAI)와 산란분포계수 (SC at TSI)는 자기공명영상 양성자 지방분율과 높은 상관성을 보였고, 지방간의 진단과 그 정도를 확인하는데 있어 높은 진단능을 보였다.

주요어 : 초음파, 간, 지방간, 정량적 영상, 비알코올성 지방간질환

학 번 : 2019-34541